

Oskarshamn site investigation

Mapping of borehole breakouts

**Processing of acoustical televiewer data
from KAV04A, KLX10, KLX11A, KLX12A,
KLX15A, and KLX18A**

Jørgen Ringgaard, Rambøll A/S

January 2009

Svensk Kärnbränslehantering AB

Swedish Nuclear Fuel
and Waste Management Co

Box 250, SE-101 24 Stockholm
Phone +46 8 459 84 00



Oskarshamn site investigation

Mapping of borehole breakouts

Processing of acoustical televiewer data from KAV04A, KLX10, KLX11A, KLX12A, KLX15A, and KLX18A

Jørgen Ringgaard, Rambøll A/S

January 2009

Keywords: Borehole breakouts, Televiewer, Deformations, Micro fallouts.

This report concerns a study which was conducted for SKB. The conclusions and viewpoints presented in the report are those of the author and do not necessarily coincide with those of the client.

Data in SKB's database can be changed for different reasons. Minor changes in SKB's database will not necessarily result in a revised report. Data revisions may also be presented as supplements, available at www.skb.se.

A pdf version of this document can be downloaded from www.skb.se

Abstract

This report presents a detection and mapping of borehole breakouts and other borehole deformations by means of processing of data from an acoustical televiwer probe. Special attention is paid to small breakouts and micro fallouts.

The registration is done in Excel-sheets in a table and a chart, which show the main azimuth of the breakouts. The charts show an obvious tendency, that the main azimuth of the breakouts and micro fallouts is found to be at 0 to 90° from magnetic north.

Due to the inclination of the boreholes, the televiwer is slightly decentralized during logging, which causes reduced data quality. But despite this, breakouts, keyseats and washouts with a certain magnitude (more than 0.1 mm), can still be mapped and classified after centralization of data by special processing routines.

Also micro fallouts (fallouts smaller than 0.1 mm) can be registered, but the mapping of these is more uncertain, as is it not possible to make specific criteria for this phenomenon. The detection has been done as a visual inspection and it is often hard to determine the area of distribution of these small structures. In some cases the micro fallouts are found to be in the entire perimeter of the borehole, but in other cases they have a main azimuth in the same direction as the breakouts.

Sammanfattning

Denne rapport redovisar förekomsten och kartering av borrhålsspjälkning och andra borrhålsdeformationer, baserat på data från en akustisk televiwersond. Särskild vikt har lagts vid mycket små borrhålsspjälkningar och mikro utfall.

Dataregistreringen är utförd i Excel-blad i tabeller och diagram, vilka illustrerar huvud-azimuth för spjälkningarna. Diagrammen visar en tydlig tendens, att huvudazimuth för spjälkning och mikro utfall finns i intervallet 0–90° från magnetisk norr.

Pga. borrhålens lutning är televiwersonden svagt decentraliserad under loggningen, vilket leder till sämre datakvalité. Trots detta är det möjligt att urskilja spjälkning, keaseats och washouts med bestämd magnitud (mer än 0,1 mm). Detta kan åstadkommas genom att centralisering kan göras genom en speciell dataprocessrutin.

Även mikro utfall (utfall mindre än 0,1 mm) kan urskiljas, men karteringen av dessa är mer osäker, då det inte är möjligt att precisera kriterium för detta. Urskiljning har kunnat göras genom visuell bedömning och ofta är det svårt att avgöra utbredningen av dessa. I några fall har mikro utfall förekommit i hela borrhålets perimeter, men i andre fall har de haft huvudazimuth i samma riktning som spjälkningen.

Contents

1	Introduction	9
2	Objective and scope	11
3	Equipment	13
4	Processing of data	15
4.1	Import and orientation	15
4.2	Alignment of images	15
4.3	Filtering and calculation of decentralization	16
4.4	Centralization of images	17
4.5	Calculation of calipers and ovality	17
4.6	Registration of breakouts and other deformations	17
4.7	Nonconformities	17
5	Description of logpanel	19
5.1	Explanation of logs	19
5.1.1	Amplitude	19
5.1.2	Caliper max position	19
5.1.3	Caliper min position	19
5.1.4	Caliper – max – Centralized – Median filtered	19
5.1.5	Caliper – mean – Centralized – Median filtered	19
5.1.6	Caliper – min – Centralized – Median filtered	19
5.1.7	Class	19
5.1.8	Cross-section – Radius – Centralized	20
5.1.9	Decentralization	20
5.1.10	Radius – Centralized	20
5.1.11	Radius – Centralized – Median filtered	20
5.1.12	Radius – Centralized – Median filtered – median	20
5.1.13	Radius – Median filtered – max	20
5.1.14	Radius – Median filtered – median	20
5.1.15	Radius – Median filtered – mean	20
5.1.16	Radius – Median filtered – min	20
5.1.17	Tool rotation	20
6	Analysis and registration of observed deformations	21
6.1	Classification of observed deformations	21
6.2	Explanation of columns in the excel-sheet	21
6.3	Examples of borehole deformations	22
6.3.1	Example of borehole breakout (BB)	22
6.3.2	Example of washout (WO)	22
6.3.3	Example of keyseat (KS)	23
6.3.4	Example of micro fallout (MF)	24
6.4	Explanation of special features in the boreholes	25
6.4.1	Tracks from decentralization	25
6.4.2	Shadows from milling process	25
6.4.3	PLEX-reinforcement	25
7	Summary and discussions	27
8	References	29
9	Appendices	31
Appendix A	List of acquisition reports	32
Appendix B	Tables and charts of depth errors	33
Appendix C	Tables and charts of registered deformations	39
Appendix D	Plot of logpanels	45

1 Introduction

Boreholes and tunnels in sedimentary formations as well as in bedrock may, during certain conditions governed by the relation between the compressive strength of the rock material and the state of stress, be exposed to spalling, often referred to as borehole breakouts, entailing that the originally circular borehole perimeter is deformed and changes its geometry to a more or less oval shape. (More exact definitions and a classification of borehole deformations of different types are given in Section 6.1.) The orientation of breakouts is governed by the stress field, such that the breakouts (ideally) occur on opposite sides of the borehole in the same bearing as that of the minor horizontal stress.

Width, length and depth of breakouts may vary within broad ranges, reflecting variations in the rock strength-/rock stress relation /Zoback et al. 1985/ and possibly also mirroring the impact of the drilling process /Ask et al. 2006/. The study of breakouts is primarily aiming at shedding light on the orientation of the stress field and its continuity. Secondly, breakouts may be used also for determination of stress magnitudes, however mainly as a supporting method.

It has previously been shown that spalling phenomena may well be identified and characterized by the analysis of acoustic televiewer images /e.g. Deltombe and Schepers, 2000, and Siddans and Worthington, 2003/. Due to the high accuracy of the acoustic televiewer method for determination of geometrical properties of the borehole, it is especially advantageous when addressing minor deformations, which may be very difficult to detect with other methods.

A pilot study aiming at investigating the potential of the acoustic televiewer method of identifying and characterizing major as well as minor borehole deformations in the rock types prevailing at Forsmark was performed during 2005 /Ask and Ask, 2006 and Ask et al. 2006/. Two subvertical core drilled boreholes, KFM01A (1,000 m long) and KFM01B (500 m) were investigated. The applicability of the method was clearly demonstrated and a range of borehole deformations of different dimensions was revealed in both boreholes. The pilot study was followed by a more extensive study by /Ringgaard, 2007/.

This document reports the results gained by processing and interpretation of acoustic televiewer data from six boreholes at Oskarshamn, which is one of the activities performed within the site investigation at Oskarshamn. The work was carried out in accordance with activity plan AP PS 400-06-160, see Table 1-1. Activity plans and method descriptions are SKB's internal controlling documents. However, for the activity presented in this report, there exists no SKB method description.

A map of the Oskarshamn investigation area with locations of the studied boreholes is presented in Figure 1-1.

Original data from the reported activity are stored in the primary database Sicada. Data are traceable in Sicada by the Activity Plan number (AP PS 400-06-160). Only data in databases are accepted for further interpretation and modelling. The data presented in this report are regarded as copies of the original data. Data in the databases may be revised, if needed. Such revisions will not necessarily result in a revision of the P-report, although the normal procedure is that major revisions entail a revision of the P-report. Minor revisions are normally presented as supplements, available at www.skb.se.

Table 1-1. Controlling document for performance of the activity.

Activity plan	Number	Version
Detection of potential borehole breakouts in boreholes KAV04A, KLX10, KLX11A, KLX12A, KLX15A and KLX18A	AP PS 400-06-160	1.0



Figure 1-1. Map with locations of the studied boreholes at the Oskarshamn investigation area.

2 Objective and scope

Efforts to map the effects of the stress in the Oskarshamn region have been done with a suite of methods. This report describes a special processing of televiewer data with attention to the effect of stress: deformations of the borehole. The mapping is done according to the SKB-document AP PS 400-06-160. An overview of the processed boreholes can be found in Table 2-1.

Table 2-1. Overview of boreholes (from SICADA).

Borehole	Length [m]	Inclination [° from hor.]	Orientation [° from GN]
KAV04A	1,004.0	-84.90	77.03
KLX10	1,001.2	-85.19	250.81
KLX11A	992.3	-76.43	89.84
KLX12A	602.3	-75.07	315.92
KLX15A	1,000.4	-54.42	198.83
KLX18A	271.4	-82	271

3 Equipment

The probe used for acquisition of data is a High Resolution Acoustical Televiewer (HiRAT) from Robertson Geologging Ltd. <http://www.geologging.com/>

The transducer is a 1.5 MHz head, which transmits the acoustic signal via a rotating acoustic mirror to the borehole wall. The strength of the reflected signal is recorded as an Amplitude log, while the first arrivals are picked and stored in a Traveltime log. Both logs are stored as images with selectable horizontal resolution from 90 to 360 pixels/revolution and a vertical resolution depending on the logging speed. The radial resolution in the recorded Traveltime is 100 ns, which equals 0.075 mm. The boreholes were logged with different selections of resolution; an overview of this is shown in Table 3-1.

The images are oriented by means of a built-in orientation unit containing a 3-axis fluxgate magnetometer as well a 3-axis accelerometer. The output from this device can also be used to calculate a deviation log for the borehole.

The probe is centralized in the borehole with two bow spring centralizers; see the picture in Figure 3-1. The applied centralizers are designated to boreholes with diameters in the range 67–100 mm.

For detailed information regarding the data acquisition with the HiRAT probe, please refer to SKB reports listed in Appendix A.



Figure 3-1. Picture of HiRAT probe.

Table 3-1. Overview of resolutions.

Borehole	Pixels/rev.	Horizontal res. [mm]	Logging speed [m/min.]	Vertical res. [mm]
KAV04A	90	2.7	10	8
KLX10	90	2.7	10	8
KLX11A	90	2.7	10	8
KLX12A	180	1.3	2.3	2
KLX15A	120	2.0	2.3	2
KLX18A	90	2.7	10	8

4 Processing of data

The final processing of the televiewer-data contains the steps described below. A lot of effort has been spent to investigate different possibilities in the processing. Only the final processing done to the delivered data is described. All processing is done in WellCAD, which is made by Advanced Logic Technology. A free reader for WellCAD documents can be downloaded on www.alt.lu.

4.1 Import and orientation

The televiewer data are recorded in the dedicated logging-program HiRAT from Robertson Geologging Ltd. The data are stored in time domain, with a table which links the data to depth.

Image-data as well as orientation-data are imported and resampled to depth-domain. Orientation-data are filtered with a 25 samples moving average filter in boreholes with 2 mm vertical resolution, respectively with a 10 samples moving average filter in boreholes with 8 mm vertical resolution. Images are resampled to 360 or 180 pixels/rev. before orientation. This is done to prevent fractures from being edged during orientation routine.

Images are then oriented to Magnetic North (MN) by means of data from the orientation unit.

4.2 Alignment of images

In order to provide a system for length calibration of different logging systems used at the site investigation, reference tracks (grooves) have been milled into the borehole wall with a specially designed tool at regular levels in all cored drilled boreholes. Regarding televiewer logging, the length calibration is conducted as follows.

First all HiRAT logs are shifted, so that the upper edge of the top-most track is aligned to the milled reference track. Then all tracks in the borehole are identified and a table is made. An example of this is shown in Table 4-1.

Also a plot of the differences is made. This is done to check the linearity of the depth error, an example of a plot is shown in Figure 4-1. The depth tables and plots of all boreholes can be found in Appendix B.

All logs are then stretched to fit the milled tracks in the borehole, which results in a perfect alignment to the tracks.

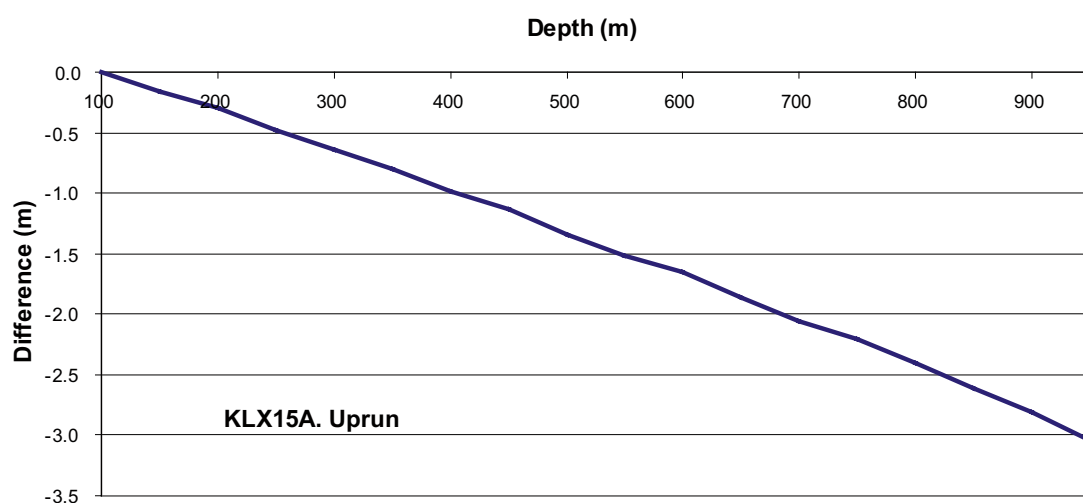


Figure 4-1. Example of plot of depth error. KLX15A.

Table 4-1 Example of depth table. KLX15A.

KLX15A. Uprun		
True depth [m]	HiRAT [m]	Difference [m]
100.000	100.000	0.000
150.000	150.155	-0.155
200.000	200.294	-0.294
250.000	250.476	-0.476
300.000	300.640	-0.640
350.000	350.803	-0.803
400.000	400.985	-0.985
450.000	451.131	-1.131
500.000	501.343	-1.343
550.000	551.521	-1.521
600.000	601.657	-1.657
650.000	651.857	-1.857
700.000	702.053	-2.053
750.000	752.207	-2.207
800.000	802.401	-2.401
850.000	852.608	-2.608
900.000	902.811	-2.811
950.000	953.039	-3.039

4.3 Filtering and calculation of decentralization

To calculate the decentralization, the Travelttime image needs to be filtered with a 15x15 pixels weighted average filter, which equals an area of 30x30 mm with 2x2 mm pixelsize. In boreholes with lower resolutions, the filter-size is reduced proportionally. This is done to prevent small fractures from disturbing the decentralization calculation. Then the image is converted from Travelttime (the unit is 100 ns) to radius with the formula:

$$Radius(mm) = \frac{(Travel\ Time - Internal\ Travelttime \times 10) \times VEL(FL)}{10 \times 1000} + tool\ radius$$

where “VEL(FL)” is the sound velocity in the borehole fluid

”Internal Travelttime” is the internal travelttime in the oil from the transducer to the acoustic window of the HiRAT tool. As the sound velocity in the oil has a small temperature coefficient, it is calculated as:

$$Internal\ Travelttime = \frac{(-2.24 \times TEMP(FL) + 1031) \times 120}{1000}$$

“TEMP(FL)” is the temperature of the water in the borehole, which was measured with a 9042 FluidRes and FluidTemp probe from Century Geophysical (see overview of acquisition reports in Appendix A). Also VEL(FL) is calculated in the reports, from the measured resistivity of the fluid.

Next step is to extract statistics from the new radius image log, which returns logs for minimum, maximum, average and median values of the radius image. From these the decentralization of the probe is calculated as:

$$Decentralization = "Radius - mean" - "Radius - min"$$

4.4 Centralization of images

Due to the inclination of the boreholes, the acoustic televiewer-probe is slightly decentralized during logging; the size of this decentralization is roughly 0.1 mm/deg. from vertical. Therefore a centralization routine is applied to compensate the images for this. This is done by means of a sine-fitting routine in WellCAD. It can be done only to the Traveltime (Radius) image, not to the Amplitude image.

4.5 Calculation of calipers and ovality

The Centralized Traveltime is then also converted to a radius image as described in 4.3 and the previous image is deleted.

Now mean, minimum and maximum calipers as well as angles (e.g. Caliper Max Position) for these can be extracted from the median filtered image log. Then the extracted angles (position logs) are filtered again with a 100 or 25 pts. (2 metre) moving average filter; this is done to smoothen the logs as only main angles are of interest.

An ovality log can now be calculated as twice the median radius minus the minimum caliper.

OVALITY - MIN = "Radius - Centralize - Median filtered - median " x 2 - "Caliper - min - Centralize - Median filtered"

This ovality log will only be reliable where some ovality is present, as it will be smeared by the fractures in the borehole as well as method introduced artefacts. It also needs to be compared with the angle logs, which should be stable in one direction, before a eventual ovality can be considered reliable.

As a manual check of the ovality, cross-section logs are generated every 20 metre, as well as right above and below breakouts (the latter are deleted again). These cross-sections have grid-circles every 0.5 mm, allowing the ovality to be visually checked, see example in Figure 4-2 below.

When necessary, the same process is applied to the downrun and imported to the uprun logpanel. It is used in case of doubt to help separating real deformations from artefacts. The Radius image is deleted again.

4.6 Registration of breakouts and other deformations

To register and describe deformations the log panel is manually inspected. When necessary a cross-section is generated and the deformation is classified, measured and registered in an Excel-table. In Figure 4-2 below is shown an example of a cross-section. The spacing between the radial grid here is 0.1 mm. The spikes on the cross-section, which have a maximum size of 0.3 mm, show some roughness on the borehole wall – micro fallout.

4.7 Nonconformities

The activity was performed in compliance with activity plan AP PS 400-06-160. This plan was made for boreholes in the Forsmark area, so it is other boreholes, but the same method.

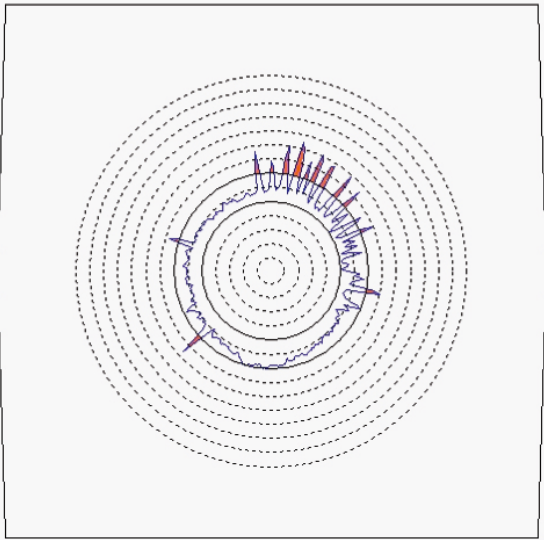


Figure 4-2. Example of cross-section with micro fallout.

5 Description of logpanel

5.1 Explanation of logs

Here follows – in alphabetic order – a description of all the logs in the panel.

5.1.1 Amplitude

Amplitude of the returned acoustic signal from the borehole wall. Darker (more blue) colours represent low amplitude – softer surface, while lighter (more yellow) colours represent high amplitude – harder surface of wall. The log is (as all other images) shown as an un-rolled 360° image of the borehole, where 0° is the reference, which is aligned against magnetic north (MN). The image has no unit.

5.1.2 Caliper max position

Orientation of the calculated maximum caliper in degrees from MN of the borehole. The log is derived from the filtered and centralized radius image. Contains values from 0–180 degrees.

5.1.3 Caliper min position

Orientation of the calculated minimum caliper in degrees from MN of the borehole. The log is derived from the filtered and centralized radius image. Contains values from 0–180 degrees.

5.1.4 Caliper – max – Centralized – Median filtered

Maximum caliper measured in the median filtered and centralized radius image. Unit: mm.

5.1.5 Caliper – mean – Centralized – Median filtered

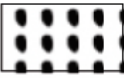

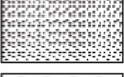
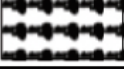
Mean caliper measured in the median filtered and centralized radius image. Unit: mm.

5.1.6 Caliper – min – Centralized – Median filtered

Minimum caliper measured in the median filtered and centralized radius image. Unit: mm.

5.1.7 Class

Symbol log, which shows the classification of registered deformations. This log is pasted from the column in the registration excel-sheet.

BB		Borehole Breakout
KS		Key Seat
MF		Micro Fallout
WO		Washout

5.1.8 Cross-section – Radius – Centralized

Cross-sections are generated every 20 metre in the borehole. The cross-section is average over 10 cm. Radii below the actual nominal radius are shaded green, and radii above are shaded orange.

5.1.9 Decentralization

Calculated decentralization as the difference between the mean and min radius of the radius image. Unit: mm.

5.1.10 Radius – Centralized

Radius image log, which is centralized as described to compensate for decentralization of the probe. Light colours represent smaller radii, while darker colours represent larger radii. Unit: mm.

5.1.11 Radius – Centralized – Median filtered

Radius image log, which is centralized as described earlier and median filtered over an area of 15x15 pixels (app. 20x30 mm) to shade for small deformations, when calculating calipers. Light colours represent smaller radii, while darker colours represent larger radii. Unit: mm.

5.1.12 Radius – Centralized – Median filtered – median

This log is not shown; it is used to calculate the ovality as described in paragraph 4.5.

5.1.13 Radius – Median filtered – max

Maximum radius of the median filtered, but not centralized radius image, unit: mm.

5.1.14 Radius – Median filtered – median

Median radius of the median filtered, but not centralized radius image, unit: mm.

5.1.15 Radius – Median filtered – mean

Mean radius of the median filtered, but not centralized radius image, unit: mm.

5.1.16 Radius – Median filtered – min

Minimum radius of the median filtered, but not centralized radius image, unit: mm.

5.1.17 Tool rotation

Shows the rotation of the probe, as the borehole was logged, unit: degrees.

6 Analysis and registration of observed deformations

6.1 Classification of observed deformations

In Appendix C is found tables with classification of all interpreted deformations in the boreholes. The classification is illustrated in Figure 6-1.

6.2 Explanation of columns in the excel-sheet

The columns in the Excel-sheet are explained as follows:

Top Depth: Top of the deformation.

Bot. Depth: Bottom of the deformation.

Max. R: Maximum radius of the deformation, read from “Radius – max – Median Filtered”-log and/or “Radius” image.

Median R: Nominal radius at the depth, read from “Radius – median – Median Filtered”-log.

dRmax: Delta radius, i.e. the depth of the deformation into the borehole wall.

Structure: Classification of the deformation. Examples and further explanation are shown in paragraph 6.3

BB: Borehole breakout

WO: Washout

KS: Key seat

MF: Micro fallout

Uncertainty: The uncertainty of the observed deformation: 3 = certain, 2 = probable, 1 = possible, 0 = not estimated. The uncertainty is primary related to the type of deformation.

Cross. struct.: The deformation is related to a fracture crossing the borehole. Example of this is shown in paragraph 6.3.

Main azimuth: Main azimuth of the deformation in degrees from Magnetic North. The angle is calculated from the next column “Azimuth”. If the angle is between 0 and 180°, the main azimuth is the same, but if the azimuth is between 180 and 360°, 180° are subtracted from the angle. Example of this is shown and explained in paragraph 6.3.

Azimuth: Angle from MN to the dominating point of the deformation.

Aperture α 1: Angle from MN to first edge of the deformation. If the deformation is located around 0° MN, this angle is noted as a negative angle from MN, e.g. -5°. This angle equals 355°.

Aperture α 2: Angle from MN to last edge of the deformation.

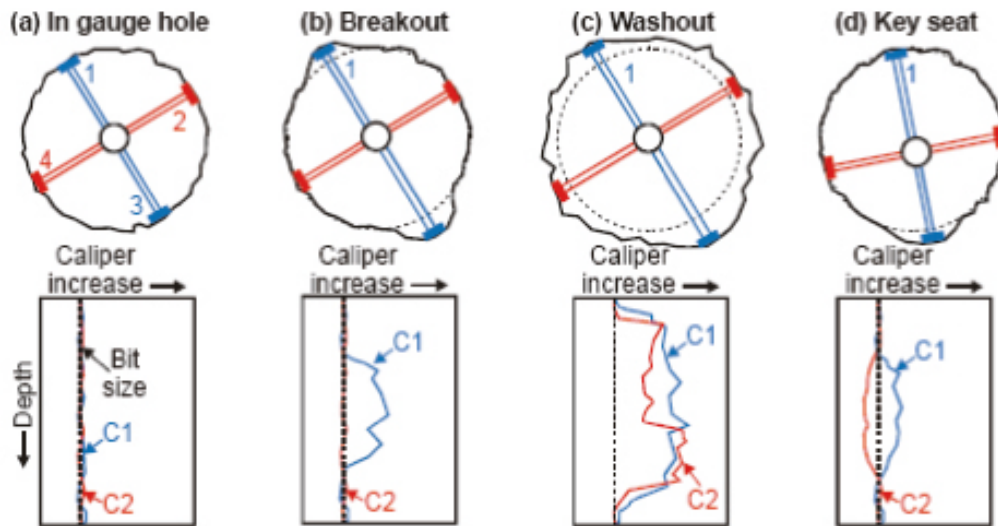


Figure 6-1. Classification of deformations. /from Ask and Ask, 2006, after Plumb and Hickman, 1985/.

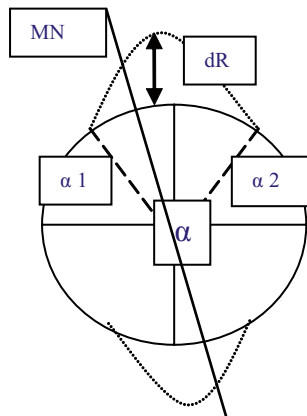


Figure 6-2. Illustration of angles.

6.3 Examples of borehole deformations

6.3.1 Example of borehole breakout (BB)

In Figure 6-3 an example of borehole breakout from KLX15A is shown. As there are obvious diametrically opposite deep fallouts, this deformation is Classified as BB with the uncertainty as “3” – most certain. As the breakout is seen to be in connection with a fracture crossing the borehole, a “Y” (Yes) is placed in the “Crossing structure” column. Here the deepest and most dominating fallout is seen at 46° and the aperture of the fallout is read to be from -10 to 45° .

The centralization routine is only perfect in a truly circular borehole. Elsewhere it adds some distortion to the centralized images, which can be seen as white (closer) areas around the fallouts. Therefore the truest picture of fallouts is seen on the “Radius”-image and the “Amplitude”-image, as these are not centralized.

6.3.2 Example of washout (WO)

In Figure 6-4 an example of washout (WO) from KLX10 is shown. Washouts are separated from breakouts, as there is fallout in the entire perimeter of the borehole, thus the minimum diameter is enlarged. Also here (if possible) a dominating azimuth and aperture angles are read and registered in the Excel sheet.

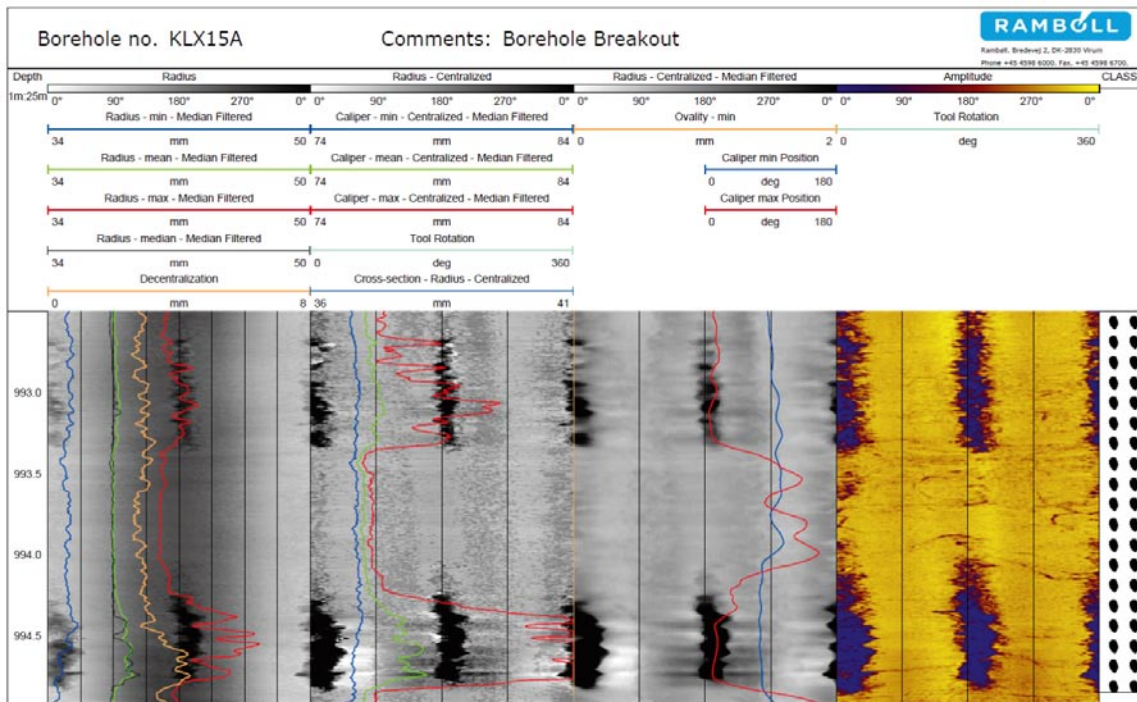


Figure 6-3. Example of breakout from KLX15A.

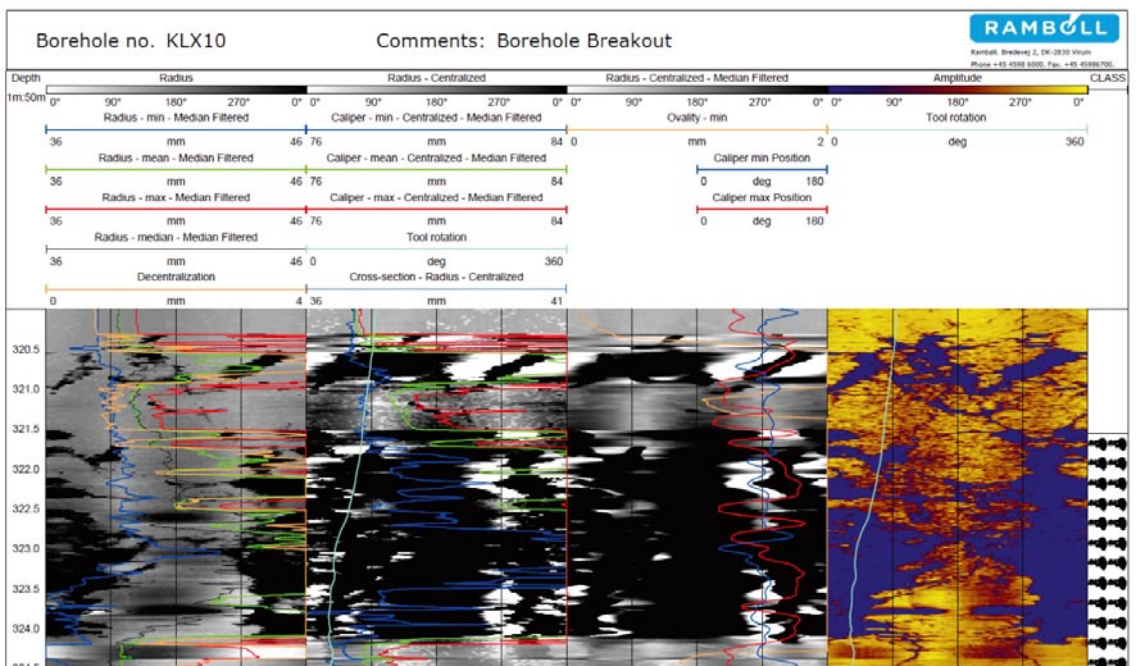


Figure 6-4. Example of washout from KLX10.

6.3.3 Example of keyseat (KS)

In Figure 6-5 an example of a keyseat (KS) from KLX12A is displayed. The keyseat recognised as fallout in only one direction at the relevant depth. Also here azimuth and aperture angles are read and registered in the Excel sheet.

6.3.4 Example of micro fallout (MF)

In Figure 6-6 an example of micro fallout is presented. In this example the micro fallout is recognized as two vertical bands in the borehole (which here ends in 205m). In these cases azimuth and aperture angles are registered. In other cases the fallout is found in the entire circumference of the borehole (with or without a dominating azimuth). In these cases the aperture angles are registered as 0 to 360°.

The micro fallout is mainly recognised on the Amplitude-image. It is sometimes hard to separate from breakouts, but a condition has been set up, that breakouts should be found also on the Radius-images as darker areas – holes. The registration of micro fallout is generally the most uncertain.

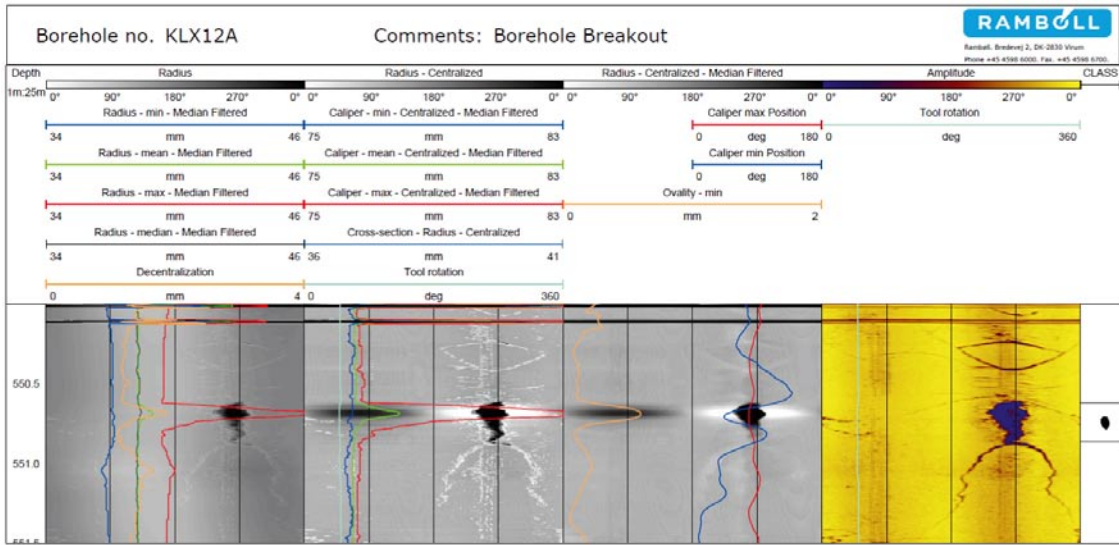


Figure 6-5. Example of keyseat from KLX12A.

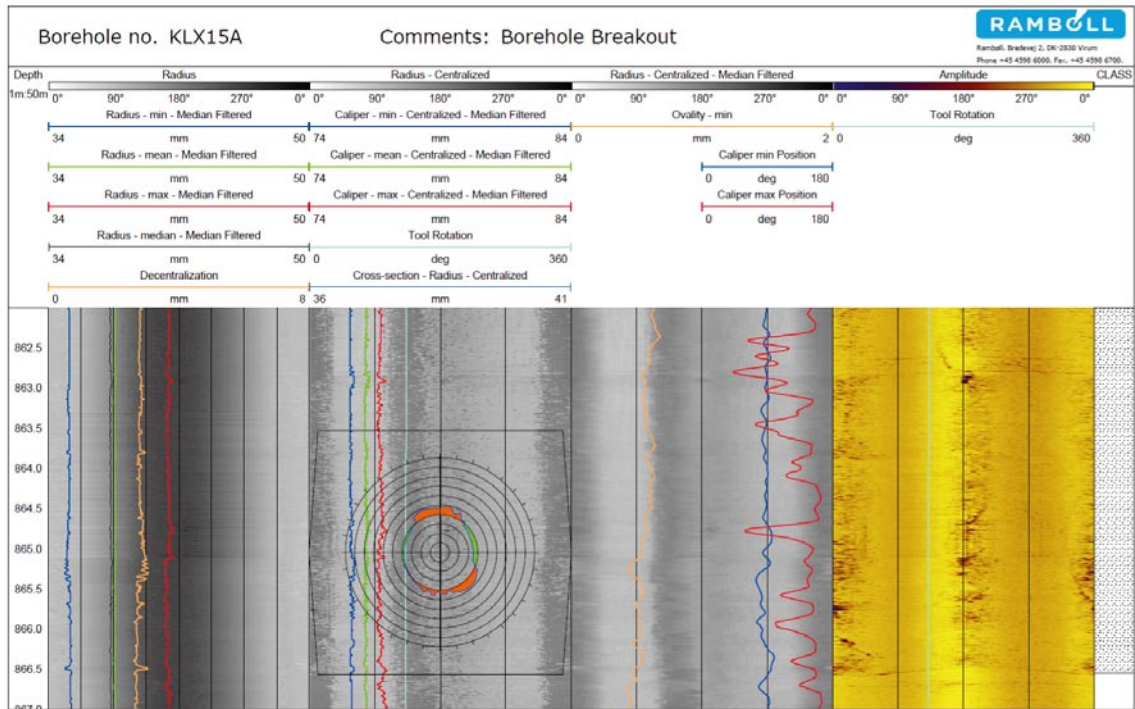


Figure 6-6. Example of micro fallout from KLX15A.

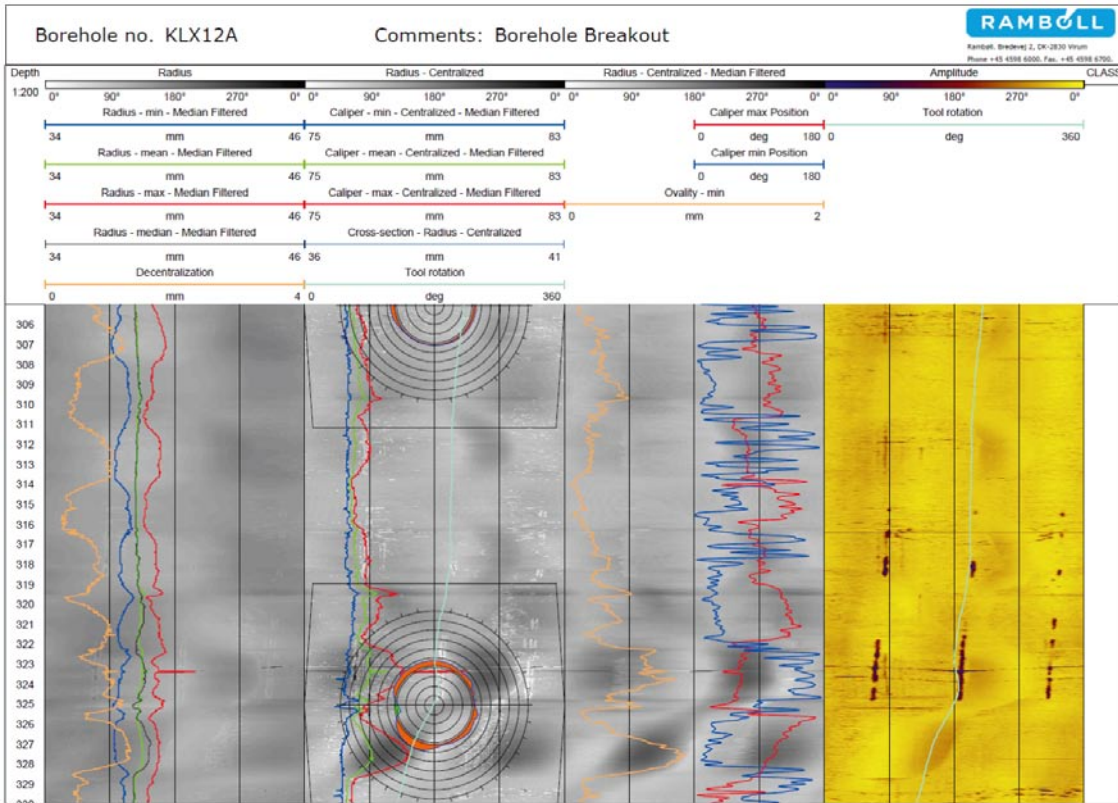


Figure 6-8. Shadows from milling.

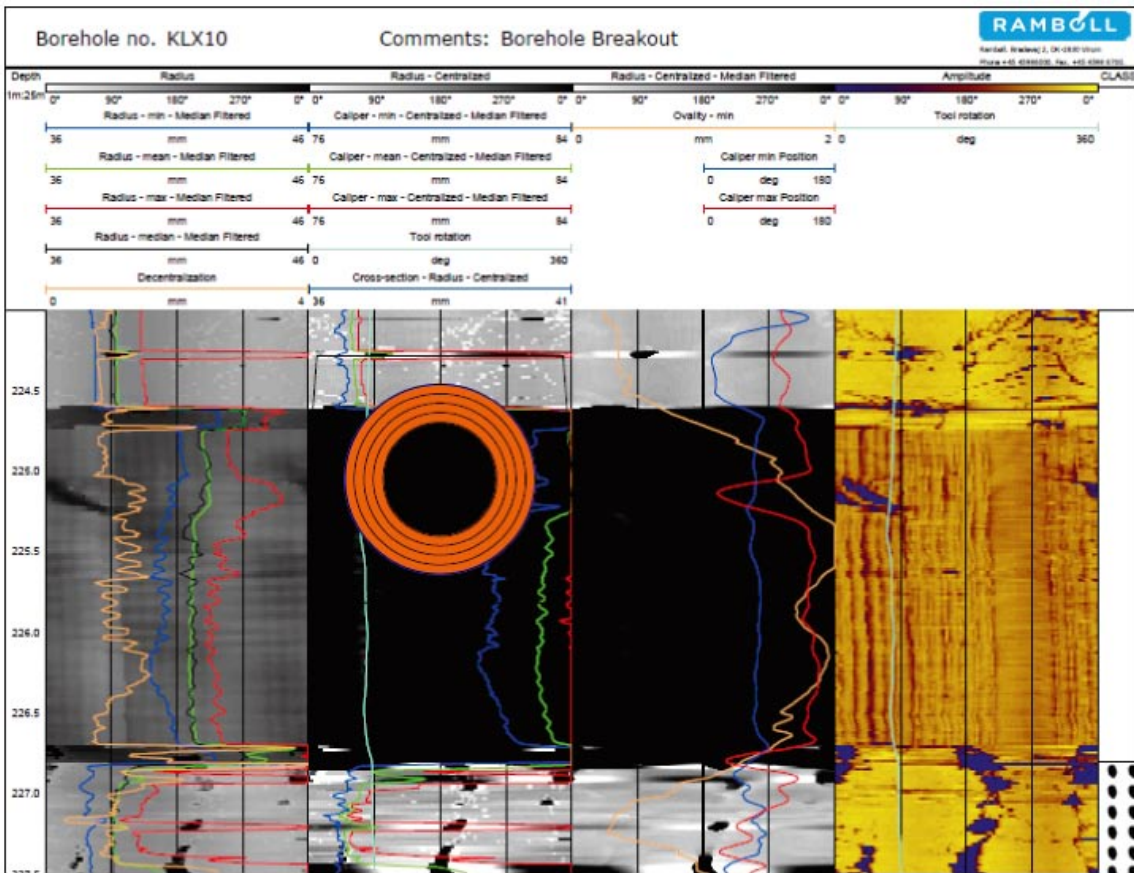


Figure 6-9. PLEX reinforcement.

7 Summary and discussions

- It is relatively fast to locate larger deformations, simply by means of scrolling through a calculated high resolution caliper.
- Orientation and size of the deformations can be precisely mapped.
- There is an obvious tendency that the main azimuth of breakouts and micro fallouts in all the boreholes is found to be at 0 to 90° from magnetic north. However the main azimuth is changing from 0–30° in KLX15A, over 25–70° in KAV04A, KLX10 and KLX11A, to 75–90° in KLX12A.
- In KLX18A only uncertain micro fallout is registered – no breakout.
- In boreholes deviated more than 10° from vertical, the cross-sections are often too disturbed or noisy from decentralization to be used.
- It is strongly recommended, that the logpanels are evaluated in WellCAD or the free WellCAD-reader, as a print-out or PDF does not provide the necessary flexibility to zoom and focus on relevant deformations.
- When smaller breakouts or micro fallout are found in connection with fractures, it can be difficult to clarify, whether the fallout was caused by the drilling process or by stress.
- The registration of micro fallout is somewhat subjective, as it is hard to quantify the propagation of it. Micro fallout which tends to have a main orientation is prioritised in the registration.

8 References

Zoback M D, Moos D, Martin L, Andersson R N, 1985. Borehole breakouts and in situ stress. *J. Geophys. Res.*, 90, pp. 5523–30.

Ask M V S, Ask D, Christiansson R, 2006. Detection of borehole breakouts at the Forsmark site, Sweden. Proc. Int. Symp. on In-Situ Rock Stress (Eds. Lu M, Li CC, Kjørholt H, Dahle H), June 19-21, 2006, Trondheim, Norway, pp. 79–86.

Deltombe J L, Schepers R, 2000. Combined Processing of BHTV Traveltime and Amplitude Images. In *Proc. Int. Symp. Borehole Geophysics for Minerals, Geotechnical, and Groundwater applications*, Golden, CO, United States, Vol. 7 pp. 29–42.

Siddans A W B, Worthington P, 2003. Structural geology using borehole wall imagery. Case studies of 3 HiRAT logs. Not published, can be found on Robertson Geologgings homepage.

Ask D, Ask M V S, 2006. Detection of potential borehole breakouts in boreholes KFM01A and KFM01B. SKB P-07–235, Svensk Kärnbränslehantering AB.

Plumb R A, Hickman S H, 1985. Stress-induced borehole elongation: A comparison between four-arm dipmeter and the borehole televiewer in the Auburn geothermal well. *J. Geophys. Res.*, 90, p. 5513–21.

Ringgard J, 2007. Mapping of borehole breakouts. Processing of acoustical televiewerdata from KFM01A, KFM01B, KFM02A, KFM03A, KFM03B, KFM04A, KFM05A, KFM06A and KFM07C. SKB P-07-07, Svensk Kärnbränslehantering AB.

9 Appendices

- A. List of acquisition reports.
- B. Plots with depth tables and errors.
- C. Tables with registered borehole deformations.
- D. Plots of WellCAD-panels from all boreholes.

List of acquisition reports

List of acquisition reports from logging with acoustic televiewer, fluid temperature and resistivity – and calculation of fluid velocity.

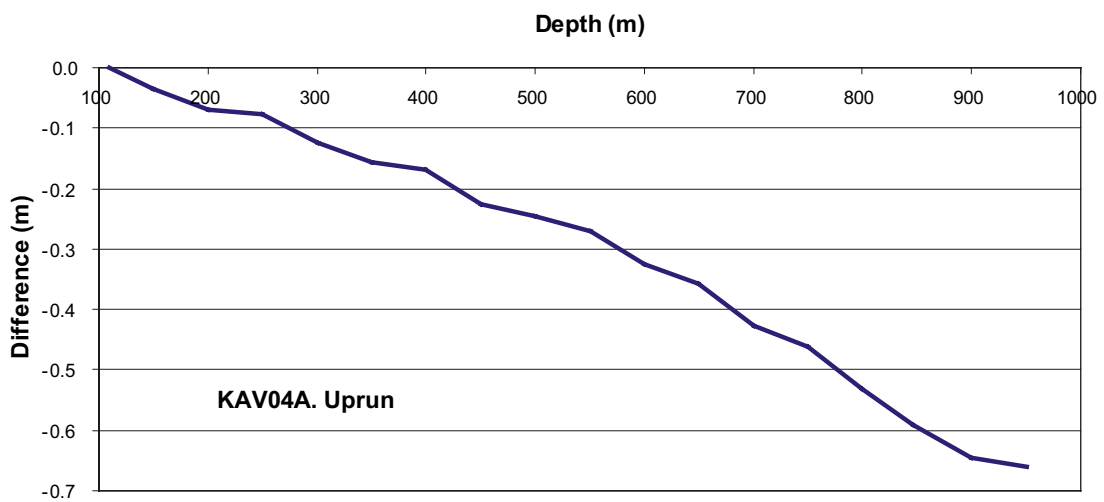
- KAV04A: SKB P-04-202. Geophysical borehole logging in borehole KAV04A, KAV04B, HLX13 and HLX15. Oskarshamn site investigation. Nielsen, Uffe Torben; Ringgaard, Jørgen. 2004.
- KLX10: SKB P-06-205. Geophysical borehole logging in borehole KLX10. Oskarshamn site investigation. Nielsen, Uffe Torben; Ringgaard, Jørgen; Dahl, Jesper Fris. 2006.
- KLX11A: SKB P-06-197. Geophysical borehole logging in borehole KLX11A, HLX36 and HLX37. Oskarshamn site investigation. Nielsen, Uffe Torben; Ringgaard, Jørgen. 2006.
- KLX12A: SKB P-06-198. Geophysical borehole logging in borehole KLX12A, KLX09G, KLX10B and KLX10C. Oskarshamn site investigation. Nielsen, Uffe Torben; Ringgaard, Jørgen. 2006.
- KLX15A: SKB P-07-152. Geophysical borehole logging in borehole KLX15A. Oskarshamn site investigation. Nielsen, Uffe Torben; Ringgaard, Jørgen. 2007.
- KLX18A: SKB P-06-290. Geophysical borehole logging in borehole KLX20A, KLX18A, KLX11B, KLX09B, KLX09D, KLX09F, HLX38, HLX39, HLX40 and HLX41. Oskarshamn site investigation. Nielsen, Uffe Torben; Ringgaard, Jørgen. 2006.

Tables and charts of depth errors

KAV04A

KAV04A. Uprun

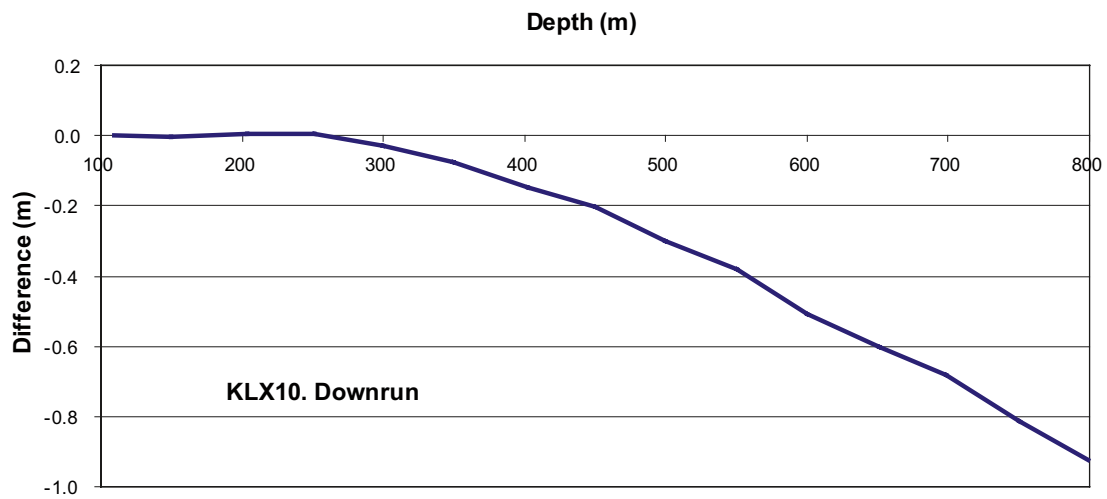
True depth [m]	HiRAT [m]	Difference [m]
110.000	110.000	0.000
150.000	150.035	-0.035
200.000	200.069	-0.069
250.000	250.077	-0.077
300.000	300.123	-0.123
350.000	350.157	-0.157
400.000	400.168	-0.168
451.000	451.226	-0.226
500.000	500.245	-0.245
550.000	550.271	-0.271
600.000	600.326	-0.326
650.000	650.358	-0.358
700.000	700.426	-0.426
750.000	750.461	-0.461
800.000	800.530	-0.530
846.000	846.590	-0.590
900.000	900.645	-0.645
950.000	950.660	-0.660



KLX10

KLX10. Downrun

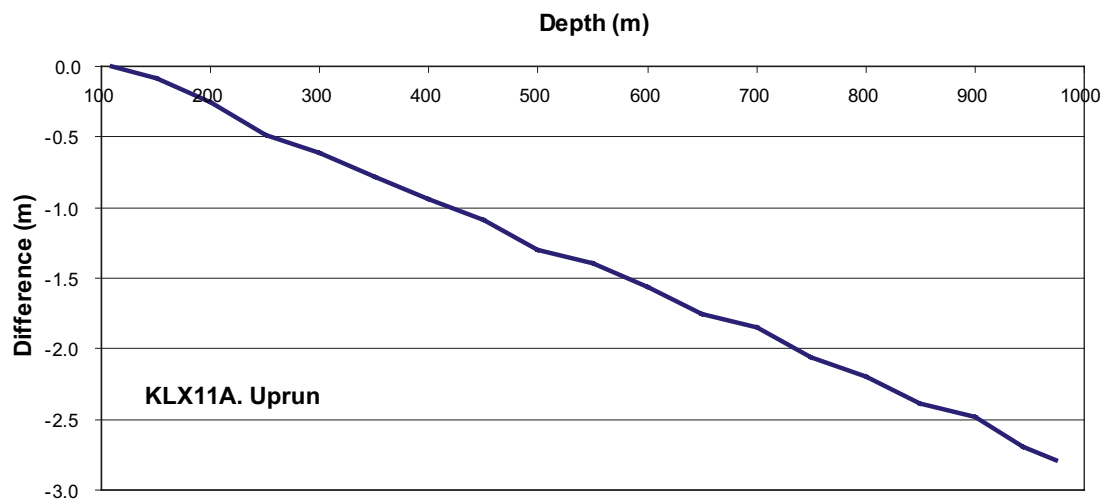
True depth [m]	HiRAT [m]	Difference [m]
110.000	110.000	0.000
150.000	150.004	-0.004
204.000	203.995	0.005
251.000	250.995	0.005
300.000	300.028	-0.028
350.000	350.076	-0.076
402.000	402.147	-0.147
450.000	450.204	-0.204
500.000	500.300	-0.300
550.000	550.380	-0.380
600.000	600.508	-0.508
651.000	651.603	-0.603
698.000	698.683	-0.683
750.000	750.812	-0.812
799.000	799.924	-0.924



KLX11A

KLX11A. Uprun

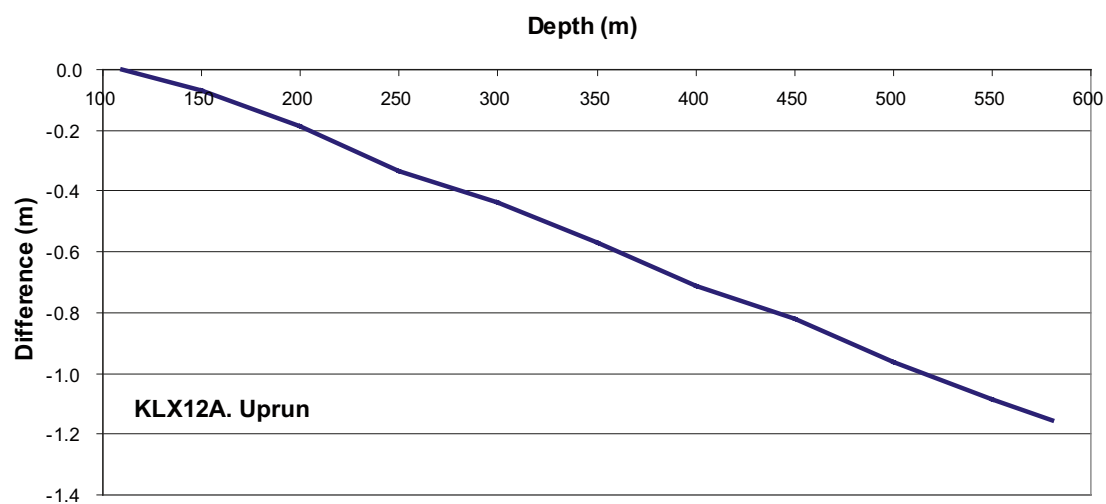
True depth [m]	HIRAT [m]	Difference [m]
110.000	110.000	0.000
150.000	150.085	-0.085
200.000	200.249	-0.249
250.000	250.489	-0.489
300.000	300.609	-0.609
350.000	350.784	-0.784
400.000	400.937	-0.937
450.000	451.088	-1.088
500.000	501.296	-1.296
550.000	551.390	-1.390
600.000	601.568	-1.568
650.000	651.750	-1.750
700.000	701.850	-1.850
750.000	752.056	-2.056
800.000	802.200	-2.200
850.000	852.390	-2.390
900.000	902.487	-2.487
944.000	946.696	-2.696
974.000	976.793	-2.793



KLX12A

KLX12A. Uprun

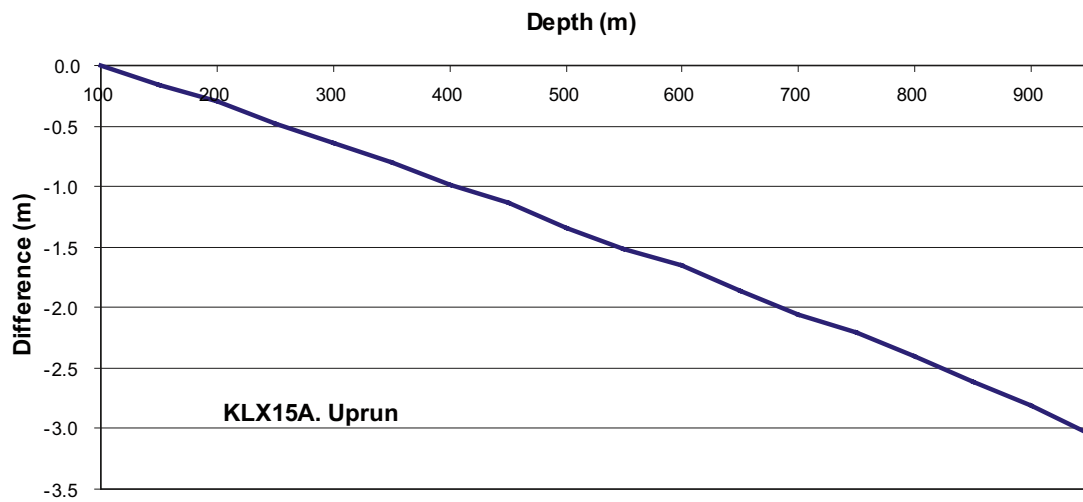
True depth [m]	HiRAT [m]	Difference [m]
110.000	110.000	0.000
150.000	150.069	-0.069
200.000	200.187	-0.187
250.000	250.333	-0.333
300.000	300.436	-0.436
350.000	350.568	-0.568
400.000	400.713	-0.713
450.000	450.822	-0.822
500.000	500.963	-0.963
550.000	551.085	-1.085
580.000	581.153	-1.153



KLX15A

KLX15A. Uprun

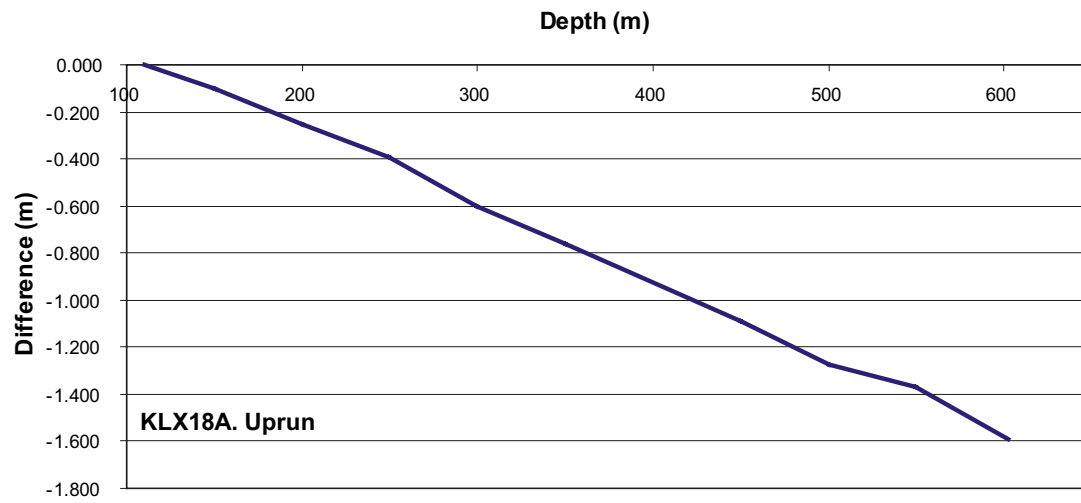
True depth [m]	HiRAT [m]	Difference [m]
100.000	100.000	0.000
150.000	150.155	-0.155
200.000	200.294	-0.294
250.000	250.476	-0.476
300.000	300.640	-0.640
350.000	350.803	-0.803
400.000	400.985	-0.985
450.000	451.131	-1.131
500.000	501.343	-1.343
550.000	551.521	-1.521
600.000	601.657	-1.657
650.000	651.857	-1.857
700.000	702.053	-2.053
750.000	752.207	-2.207
800.000	802.401	-2.401
850.000	852.608	-2.608
900.000	902.811	-2.811
950.000	953.039	-3.039



KLX18A

KLX18A. Uprun

True depth [m]	HiRAT [m]	Difference [m]
110.000	110.000	0.000
150.000	150.104	-0.104
200.000	200.256	-0.256
250.000	250.392	-0.392
300.000	300.604	-0.604
350.000	350.759	-0.759
450.000	451.087	-1.087
500.000	501.271	-1.271
550.000	551.368	-1.368
602.000	603.592	-1.592

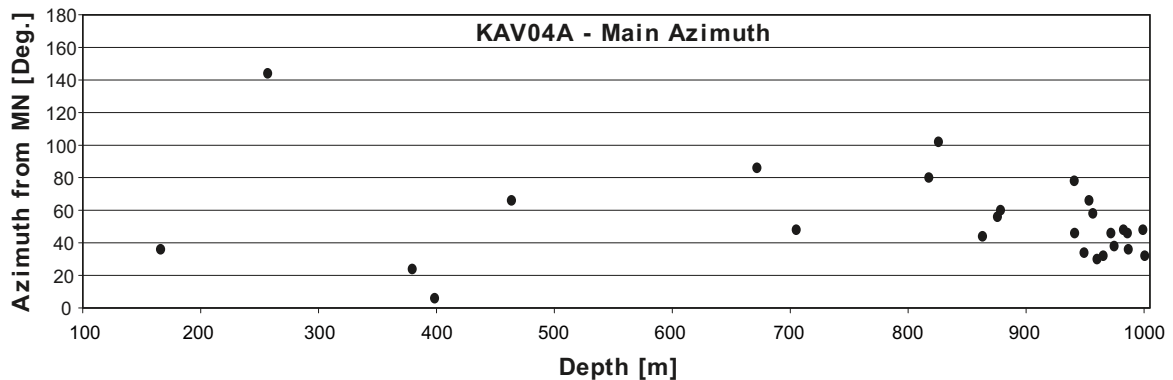


Tables and charts of registered deformations

KAV04A

KAV04A – Observed BB, WO, MF and KS

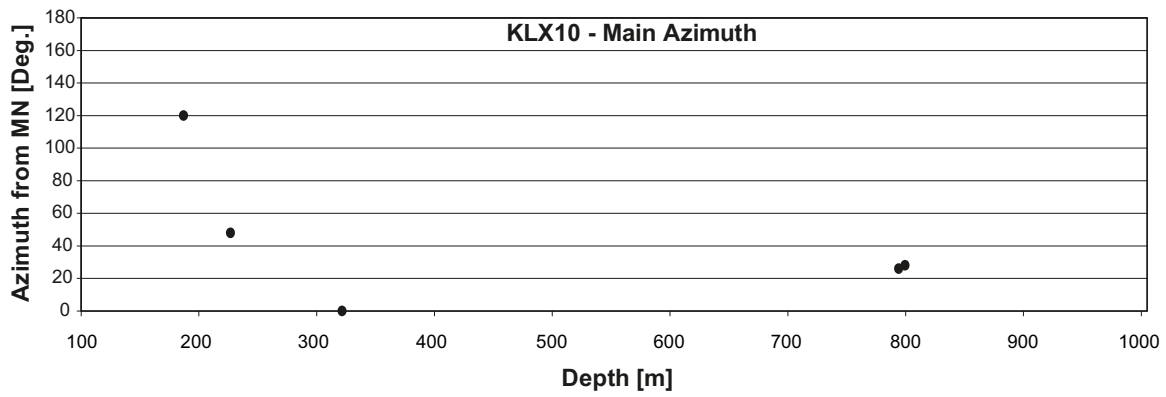
Top Depth	Bot. depth	Max R	Median R	dRmax	Class	Uncertainty	Cross-struct.	Main Azimuth	Azi-muth	Aperture α1	Aperture α2	Comments
[m]	[m]	[mm]	[mm]	[mm]		[0–3]	[Yes/No]	[Deg. from MN]	[Deg. from MN]	[Deg. from MN]	[Deg. from MN]	
166.10	166.35	38.1	38.1	0.1	MF	2	Y	36	36	-40	80	
255.55	256.87	41.0	37.8	3.2	MF	3	Y			0	360	
256.87	257.03	45.0	37.8	7.2	BB	2	Y	144	324	296	360	
257.03	257.37	41.4	37.8	3.6	MF	3	N			0	360	
353.98	357.72	38.0	37.8	0.2	MF	2	N			0	360	
379.47	379.59	38.4	38.0	0.4	KS	1	N	24	24	0	52	
398.50	398.57	39.3	38.0	1.3	KS	2	N	6	186	182	206	
463.70	463.76	42.8	37.9	4.9	KS	3	N	66	66	12	118	
671.83	671.93	41.0	38.2	2.8	KS	3	N	86	266	294	326	
705.10	705.30	38.6	38.0	0.6	BB	2	Y	48	48	14	78	
817.50	817.78	38.6	38.3	0.3	BB	1	Y	80	80	56	102	
825.67	826.73	39.3	38.3	1.0	BB	2	Y	102	102	78	124	
863.04	865.56	41.0	38.0	3.0	BB	1	Y	44	224	180	270	
875.76	875.92	39.5	38.2	1.3	BB	2	Y	56	236	214	258	
878.34	881.29	38.4	38.2	0.2	MF	2	Y	60	240	180	284	
940.96	941.18	38.3	37.9	0.4	BB	3	N	78	78	56	96	
941.26	943.34	39.8	38.0	1.8	BB	2	Y	46	46	28	64	
949.19	950.24	39.8	37.9	1.9	BB	2	Y	34	214	202	250	
953.36	954.18	42.3	37.8	4.5	BB	3	N	66	66	32	100	
956.63	956.76	40.8	37.8	3.0	BB	2	N	58	58	44	70	
960.25	965.13	40.0	37.8	2.2	MF	3	N	30	30	0	68	
965.47	969.59	43.5	37.8	5.7	BB	3	N	32	32	0	76	
971.89	973.18	43.0	37.9	5.1	BB	3	N	46	226	194	272	
974.70	974.78	43.0	38.0	5.0	BB	3	Y	38	38	10	70	
982.59	986.00	38.0	37.8	0.2	MF	3	N	48	228	192	260	
986.00	986.72	43.5	37.8	5.7	BB	3	N	46	46	20	72	
986.72	999.00	42.0	37.8	4.2	MF	3	N	36	36	10	70	
999.10	999.60	41.2	37.7	3.5	BB	3	N	48	48	-20	65	
1,000.60	1,002.33	51.0	37.8	13.2	BB	3	N	32	32	0	78	



KLX10

KLX10 – Observed BB, WO, MF and KS

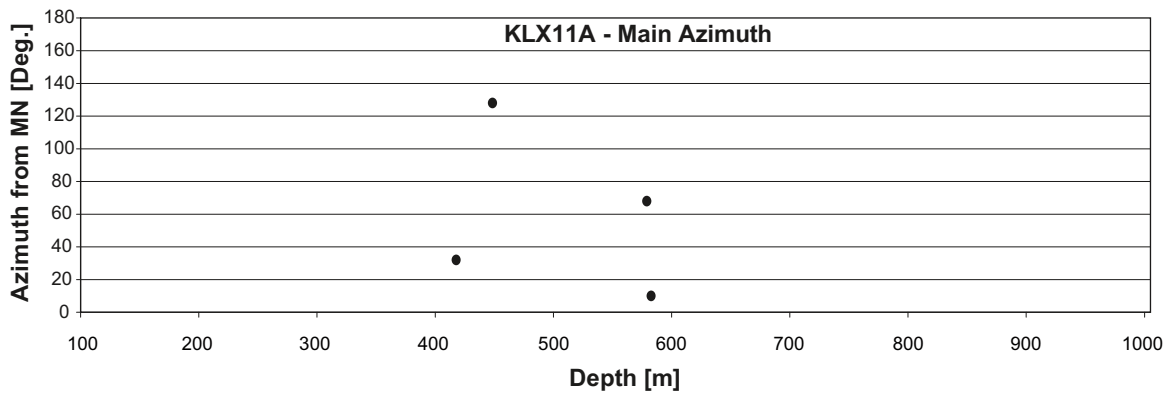
Top Depth [m]	Bot. depth [m]	Max R [mm]	Median R [mm]	dRmax [mm]	Class	Uncertainty [0–3]	Cross-struct. [Yes/No]	Main Azimuth [Deg. from MN]	Azi-muth [Deg. from MN]	Aperture α_1 [Deg. from MN]	Aperture α_2 [Deg. from MN]	Comments
150.30	161.50	38.6	38.5	0.1	MF	2	N			0	360	
187.00	205.05	100.0	38.5	61.5	BB	2	Y	120	120	74	180	Several small
226.80	232.50	75.0	38.6	36.4	BB	1	Y	48	228	64	180	
321.56	327.36	120.0	38.7	81.3	WO	1	Y	0	0	-90	90	
794.12	799.59	39.0	38.9	0.1	MF	3	N	26	26	-10	80	
799.60	802.40	48.0	38.9	9.1	BB	3	Y	28	28	8	50	



KLX11A

KLX11A – Observed BB, WO, MF and KS

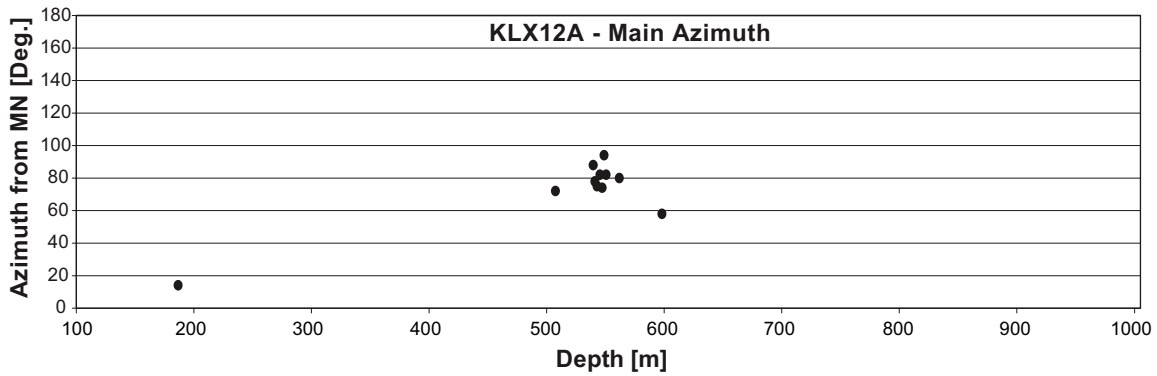
Top Depth	Bot. depth	Max R	Median R	dRmax	Class	Uncertainty	Cross-struct.	Main Azimuth	Azimuth	Aperture α_1	Aperture α_2	Comments
[m]	[m]	[mm]	[mm]	[mm]		[0-3]	[Yes/No]	[Deg. from MN]	[Deg. from MN]	[Deg. from MN]	[Deg. from MN]	
417.80	418.25	47.0	39.2	7.8	BB	3	N	32	212	180	270	
448.58	448.94	100.0	39.0	61.0	KS	1	Y	128	308	270	360	
579.07	579.19	42.0	39.3	2.7	BB	2	Y	68	68	50	84	
582.70	582.80	61.0	39.2	21.8	KS	2	Y	10	10	-10	30	



KLX12A

KLX12A – Observed BB, WO, MF and KS

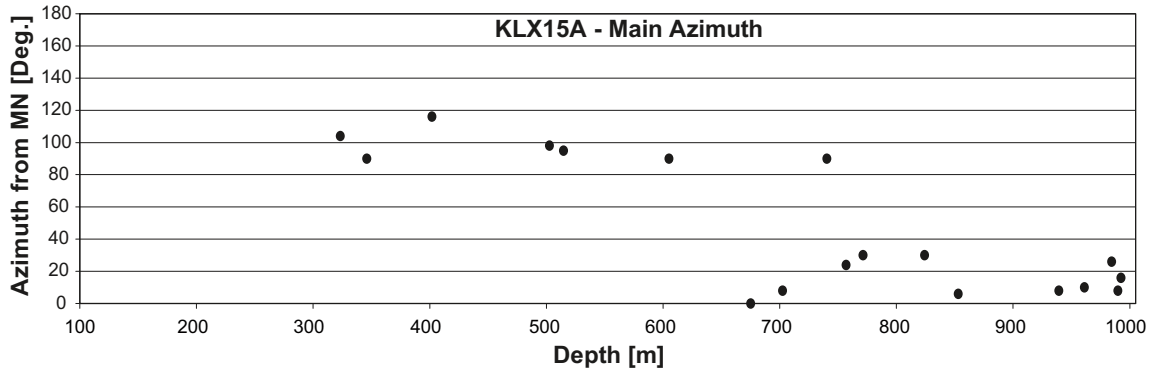
Top Depth [m]	Bot. depth [m]	Max R [mm]	Median R [mm]	dRmax [mm]	Class	Uncertainty [0–3]	Cross-struct. [Yes/No]	Main Azimuth [Deg. from MN]	Azimuth [Deg. from MN]	Aperture α_1 [Deg. from MN]	Aperture α_2 [Deg. from MN]	Comments
186.70	186.96	41.0	38.0	3.0	KS	2	Y	14	14	2	30	
507.65	507.72	43.0	38.4	4.6	KS	2	Y	72	72	24	100	
539.67	540.12	38.4	38.3	0.1	MF	3	N	88	88	28	124	
541.05	542.95	38.4	38.3	0.1	MF	3	N	78	78	40	116	
542.96	545.40	46.0	38.2	7.8	BB	3	N	75	75	44	100	
545.41	546.04	38.3	38.2	0.1	MF	3	N	82	82	44	114	
547.18	548.91	38.3	38.2	0.1	MF	3	N	74	74	44	104	
548.95	549.65	47.0	38.2	8.8	BB	3	N	94	94	62	114	
550.62	550.86	46.0	38.2	7.8	KS	3	N	82	262	234	282	
561.92	573.62	38.3	38.2	0.1	MF	2	N	80	80	48	102	
598.16	599.78	38.3	38.2	0.1	MF	2	N	58	58	0	360	



KLX15A

KLX15A – Observed BB, WO, MF and KS

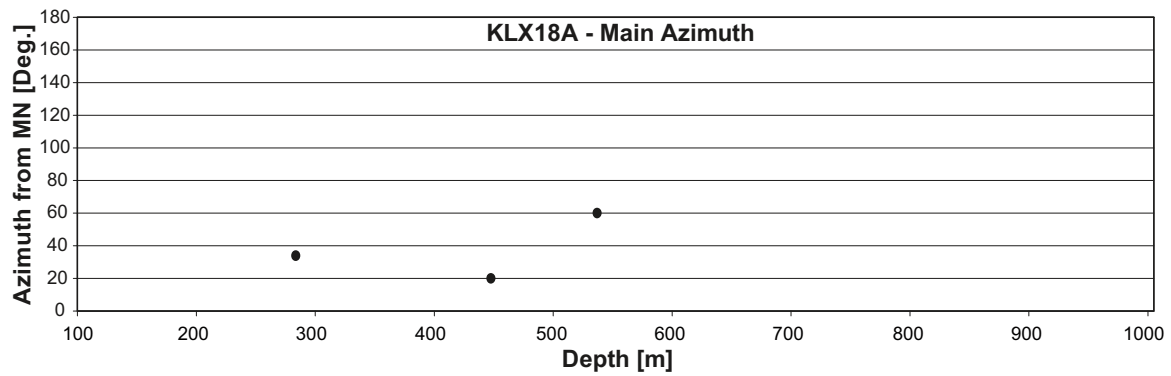
Top Depth [m]	Bot. depth [m]	Max R [mm]	Median R [mm]	dRmax [mm]	Class	Uncertainty [0–3]	Cross-struct. [Yes/No]	Main Azimuth [Deg. from MN]	Azimuth [Deg. from MN]	Aperture α_1 [Deg. from MN]	Aperture α_2 [Deg. from MN]	Comments
323.38	329.29	37.9	37.8	0.1	MF	2	N	104	284	214	334	
346.12	391.33	37.9	37.8	0.1	MF	2	N	90	270	200	336	
401.95	403.91	37.9	37.8	0.1	MF	1	N	116	296	216	344	
502.71	505.65	38.0	37.9	0.1	MF	1	N	98	278	200	336	
514.68	516.63	38.0	37.9	0.1	MF	1	N	95	275	204	360	
605.04	607.98	38.0	37.9	0.1	MF	1	N	90	270	180	360	
632.15	635.08	38.4	38.3	0.1	MF	2	N			0	360	
675.13	676.07	39.5	38.0	1.5	BB	3	N	0	180	156	198	
681.18	682.77	38.1	38.0	0.1	MF	2	N			0	360	
702.49	704.96	38.1	38.0	0.1	MF	1	N	8	8	-30	34	
740.40	747.53	38.0	37.9	0.1	MF	1	N	90	270	210	360	
756.85	770.40	38.0	37.9	0.1	MF	3	N	24	24	-10	64	
771.49	771.99	40.0	38.0	2.0	BB	3	N	30	30	14	48	
824.20	845.83	38.0	37.9	0.1	MF	2	N	30	30	-20	54	
853.00	866.55	38.0	37.9	0.1	MF	2	N	6	6	-30	34	
939.22	940.55	42.0	38.0	4.0	BB	3	N	8	8	-25	34	
961.24	985.00	38.0	37.9	0.1	MF	3	N	10	10	-20	40	
984.47	985.81	42.0	37.8	4.2	BB	3	N	26	26	5	50	
989.91	992.32	38.2	37.8	0.4	MF	3	N	8	8	-20	25	
992.50	994.85	46.0	37.9	8.1	BB	3	N	16	16	-10	45	



KLX18A

KLX18A – Observed BB, WO, MF and KS

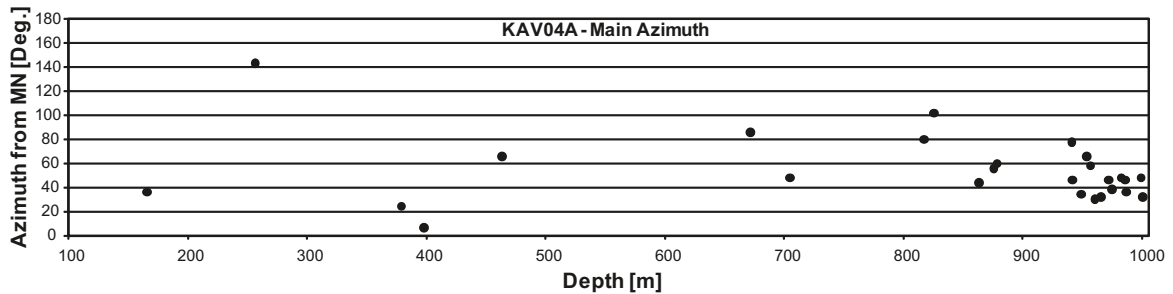
Top Depth [m]	Bot. depth [m]	Max R [mm]	Median R [mm]	dRmax [mm]	Class	Uncertainty [0–3]	Cross-struct. [Yes/No]	Main Azimuth [Deg. from MN]	Azimuth [Deg. from MN]	Aperture α_1 [Deg. from MN]	Aperture α_2 [Deg. from MN]	Comments
283.70	289.64	38.4	38.3	0.1	MF	2	N	34	34	-40	72	
447.75	458.56	38.4	38.3	0.1	MF	1	N	20	20	0	80	
537.00	540.50	38.5	38.4	0.1	MF	1	N	60	60	10	100	



Plot of logpanels

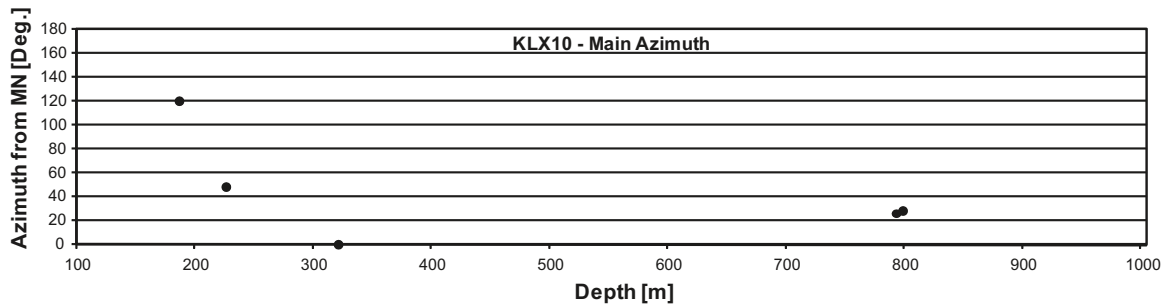
KAV04A – Observed BB, WO, MF and KS

Top Depth [m]	Bot. depth [m]	Max R [mm]	Median R [mm]	dRmax [mm]	Class	Uncertainty [0-3]	Cross-struct. [Yes/No]	Main Azimuth [Deg. from MN]	Azimuth [Deg. from MN]	Aperture α 1 [Deg. from MN]	Aperture α 2 [Deg. from MN]	Comments
166.10	166.35	38.1	38.1	0.1	MF	2	Y	36	36	-40	80	
255.55	256.87	41.0	37.8	3.2	MF	3	Y			0	360	
256.87	257.03	45.0	37.8	7.2	BB	2	Y	144	324	296	360	
257.03	257.37	41.4	37.8	3.6	MF	3	N			0	360	
353.98	357.72	38.0	37.8	0.2	MF	2	N			0	360	
379.47	379.59	38.4	38.0	0.4	KS	1	N	24	24	0	52	
398.50	398.57	39.3	38.0	1.3	KS	2	N	6	186	182	206	
463.70	463.76	42.8	37.9	4.9	KS	3	N	66	66	12	118	
671.83	671.93	41.0	38.2	2.8	KS	3	N	86	266	294	326	
705.10	705.30	38.6	38.0	0.6	BB	2	Y	48	48	14	78	
817.50	817.78	38.6	38.3	0.3	BB	1	Y	80	80	56	102	
825.67	826.73	39.3	38.3	1.0	BB	2	Y	102	102	78	124	
863.04	865.56	41.0	38.0	3.0	BB	1	Y	44	224	180	270	
875.76	875.92	39.5	38.2	1.3	BB	2	Y	56	236	214	258	
878.34	881.29	38.4	38.2	0.2	MF	2	Y	60	240	180	284	
940.96	941.18	38.3	37.9	0.4	BB	3	N	78	78	56	96	
941.26	943.34	39.8	38.0	1.8	BB	2	Y	46	46	28	64	
949.19	950.24	39.8	37.9	1.9	BB	2	Y	34	214	202	250	
953.36	954.18	42.3	37.8	4.5	BB	3	N	66	66	32	100	
956.63	956.76	40.8	37.8	3.0	BB	2	N	58	58	44	70	
960.25	965.13	40.0	37.8	2.2	MF	3	N	30	30	0	68	
965.47	969.59	43.5	37.8	5.7	BB	3	N	32	32	0	76	
971.89	973.18	43.0	37.9	5.1	BB	3	N	46	226	194	272	
974.70	974.78	43.0	38.0	5.0	BB	3	Y	38	38	10	70	
982.59	986.00	38.0	37.8	0.2	MF	3	N	48	228	192	260	
986.00	986.72	43.5	37.8	5.7	BB	3	N	46	46	20	72	
986.72	999.00	42.0	37.8	4.2	MF	3	N	36	36	10	70	
999.10	999.60	41.2	37.7	3.5	BB	3	N	48	48	-20	65	
1,000.60	1,002.33	51.0	37.8	13.2	BB	3	N	32	32	0	78	



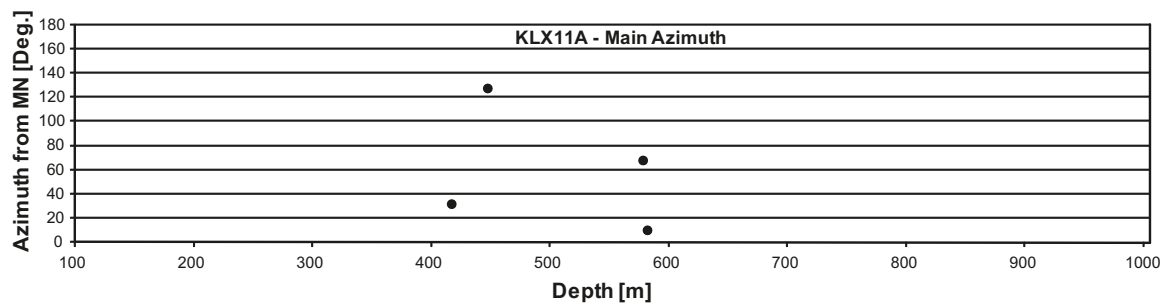
KLX10 – Observed BB, WO, MF and KS

Top Depth [m]	Bot. depth [m]	Max R [mm]	Median R [mm]	dRmax [mm]	Class	Uncertainty [0–3]	Cross-struct. [Yes/No]	Main Azimuth [Deg. from MN]	Azimuth [Deg. from MN]	Aperture α_1 [Deg. from MN]	Aperture α_2 [Deg. from MN]	Comments
150.30	161.50	38.6	38.5	0.1	MF	2	N			0	360	
187.00	205.05	100.0	38.5	61.5	BB	2	Y	120	120	74	180	Several small
226.80	232.50	75.0	38.6	36.4	BB	1	Y	48	228	64	180	
321.56	327.36	120.0	38.7	81.3	WO	1	Y	0	0	-90	90	
794.12	799.59	39.0	38.9	0.1	MF	3	N	26	26	-10	80	
799.60	802.40	48.0	38.9	9.1	BB	3	Y	28	28	8	50	



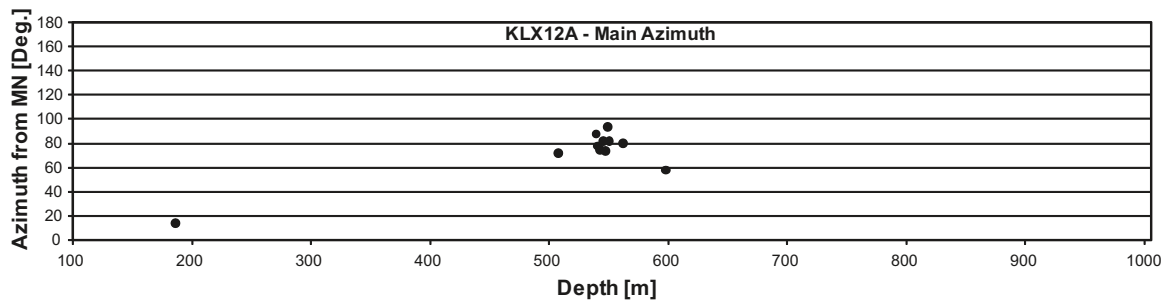
KLX11A – Observed BB, WO, MF and KS

Top Depth [m]	Bot. depth [m]	Max R [mm]	Median R [mm]	dRmax [mm]	Class	Uncertainty [0–3]	Cross-struct. [Yes/No]	Main Azimuth [Deg. from MN]	Azimuth [Deg. from MN]	Aperture α_1 [Deg. from MN]	Aperture α_2 [Deg. from MN]	Comments
417.80	418.25	47.0	39.2	7.8	BB	3	N	32	212	180	270	
448.58	448.94	100.0	39.0	61.0	KS	1	Y	128	308	270	360	
579.07	579.19	42.0	39.3	2.7	BB	2	Y	68	68	50	84	
582.70	582.80	61.0	39.2	21.8	KS	2	Y	10	10	-10	30	



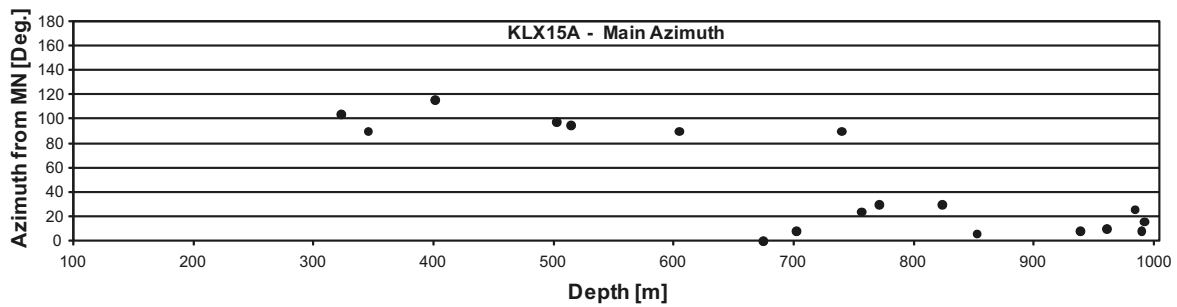
KLX12A – Observed BB, WO, MF and KS

Top Depth [m]	Bot. depth [m]	Max R [mm]	Median R [mm]	dRmax [mm]	Class	Uncertainty [0–3]	Cross-struct. [Yes/No]	Main Azimuth [Deg. from MN]	Azimuth [Deg. from MN]	Aperture α_1 [Deg. from MN]	Aperture α_2 [Deg. from MN]	Comments
186.70	186.96	41.0	38.0	3.0	KS	2	Y	14	14	2	30	
507.65	507.72	43.0	38.4	4.6	KS	2	Y	72	72	24	100	
539.67	540.12	38.4	38.3	0.1	MF	3	N	88	88	28	124	
541.05	542.95	38.4	38.3	0.1	MF	3	N	78	78	40	116	
542.96	545.40	46.0	38.2	7.8	BB	3	N	75	75	44	100	
545.41	546.04	38.3	38.2	0.1	MF	3	N	82	82	44	114	
547.18	548.91	38.3	38.2	0.1	MF	3	N	74	74	44	104	
548.95	549.65	47.0	38.2	8.8	BB	3	N	94	94	62	114	
550.62	550.86	46.0	38.2	7.8	KS	3	N	82	262	234	282	
561.92	573.62	38.3	38.2	0.1	MF	2	N	80	80	48	102	
598.16	599.78	38.3	38.2	0.1	MF	2	N	58	58	0	360	



KLX15A – Observed BB, WO, MF and KS

Top Depth [m]	Bot. depth [m]	Max R [mm]	Median R [mm]	dRmax [mm]	Class	Uncertainty [0–3]	Cross-struct. [Yes/No]	Main Azimuth [Deg. from MN]	Azimuth [Deg. from MN]	Aperture α_1 [Deg. from MN]	Aperture α_2 [Deg. from MN]	Comments
323.38	329.29	37.9	37.8	0.1	MF	2	N	104	284	214	334	
346.12	391.33	37.9	37.8	0.1	MF	2	N	90	270	200	336	
401.95	403.91	37.9	37.8	0.1	MF	1	N	116	296	216	344	
502.71	505.65	38.0	37.9	0.1	MF	1	N	98	278	200	336	
514.68	516.63	38.0	37.9	0.1	MF	1	N	95	275	204	360	
605.04	607.98	38.0	37.9	0.1	MF	1	N	90	270	180	360	
632.15	635.08	38.4	38.3	0.1	MF	2	N			0	360	
675.13	676.07	39.5	38.0	1.5	BB	3	N	0	180	156	198	
681.18	682.77	38.1	38.0	0.1	MF	2	N			0	360	
702.49	704.96	38.1	38.0	0.1	MF	1	N	8	8	-30	34	
740.40	747.53	38.0	37.9	0.1	MF	1	N	90	270	210	360	
756.85	770.40	38.0	37.9	0.1	MF	3	N	24	24	-10	64	
771.49	771.99	40.0	38.0	2.0	BB	3	N	30	30	14	48	
824.20	845.83	38.0	37.9	0.1	MF	2	N	30	30	-20	54	
853.00	866.55	38.0	37.9	0.1	MF	2	N	6	6	-30	34	
939.22	940.55	42.0	38.0	4.0	BB	3	N	8	8	-25	34	
961.24	985.00	38.0	37.9	0.1	MF	3	N	10	10	-20	40	
984.47	985.81	42.0	37.8	4.2	BB	3	N	26	26	5	50	
989.91	992.32	38.2	37.8	0.4	MF	3	N	8	8	-20	25	
992.50	994.85	46.0	37.9	8.1	BB	3	N	16	16	-10	45	



KLX18A – Observed BB, WO, MF and KS

Top Depth [m]	Bot. depth [m]	Max R [mm]	Median R [mm]	dRmax [mm]	Class	Uncertainty [0-3]	Cross-struct. [Yes/No]	Main Azimuth [Deg. from MN]	Azimuth [Deg. from MN]	Aperture α_1 [Deg. from MN]	Aperture α_2 [Deg. from MN]	Comments
283.70	289.64	38.4	38.3	0.1	MF	2	N	34	34	-40	72	
447.75	458.56	38.4	38.3	0.1	MF	1	N	20	20	0	80	
537.00	540.50	38.5	38.4	0.1	MF	1	N	60	60	10	100	

